A momentum-integral solution for flow in a rotating circular duct

John W. Chew
Design Sciences Group, Rolls-Royce plc, Derby, UK

Fully developed, incompressible, turbulent flow in a duct rotating about an orthogonal axis is considered. An integral technique, previously applied to rotating disc flows, is applied to the boundary layers, and this is patched to an approximate solution for the inviscid region of the flow. Limiting solutions are derived for $1 \ll \varepsilon \ll R$ and $1 \ll 1/\varepsilon \ll R$, where ε and R are Rossby and Reynolds numbers, respectively. In the former case, the friction factor is predicted to be proportional to $1/\varepsilon^{0.1} R^{0.2}$, which is consistent with Ito and Nanbu's (1971) measurements. Numerical solutions of the integral equations are compared with Ito and Nanbu's velocity and pressure measurements.

Keywords: integral method; turbulent flow; rotating duct

1. Introduction

The problem of flow and heat transfer in a duct rotating about an orthogonal axis is relevant to gas turbine blade cooling, and the theoretical study of such flows has received considerable attention recently. Effort has been concentrated on the numerical solution of the Reynolds-averaged Navier–Stokes equations with some model of turbulence (e.g., Iacovides and Launder 1987; Taylor et al. 1991). In the present contribution an alternative theoretical technique, the integral method, is applied. The objectives of this work are to clarify the influence of rotation on duct flow and to assess the integral method for further use.

A schematic of the secondary flow structure for the problem considered and the coordinate system used are shown in Figure 1. The Coriolis force leads to a secondary flow from the leading to the trailing edge of the tube across the central core; this mass flux is balanced by flow in the opposite direction in boundary layers adjacent to the tube wall. The flow is characterized by a Reynolds number R and Rossby number ε, defined by

$$R = dw_m/\nu, \quad \varepsilon = w_m/\Omega d \tag{1}$$

where d, w_m, ν, and Ω denote duct diameter, mean axial velocity, kinematic viscosity, and rotational speed, respectively.

An interesting analogy between rotating duct flow and rotating disc flows occurs in the limiting case $\varepsilon \ll 1$. Benton and Boyer's (1966) analytical solution for laminar flow is analogous to the Ekman boundary-layer solution that applies to many disc flows (see, e.g., Greenspan 1968). Similarly, an analytical solution of the momentum-integral equations for turbulent flow will be derived below for $\varepsilon \ll 1$, and this solution is analogous to Owen et al.'s (1985) turbulent Ekman-layer solution. Although this analogy cannot be applied directly to engine conditions, for which the Rossby number is generally greater than unity, it does suggest that the integral methods that have proved useful for disc flows (see, e.g., Chew 1990) might also be appropriate for rotating duct flows.

Address reprint requests to Dr. Chew at the Design Sciences Group, Rolls-Royce plc, Derby, UK.

Received 26 November 1991, accepted 10 October 1992

Integral methods have previously been applied to flow in a rotating circular duct by Mori and Nakayama (1968) and Ito and Nanbu (1971) for the laminar case, and by Mori et al. (1971) for the turbulent case. Mori and his coworkers report agreement between theory and their own data, but Morris (1981) has noted some discrepancies with other data. Ito and Nanbu report fair agreement between their theory and measurements for laminar flow. In the light of other theoretical work and Ito and Nanbu's measurements, Mori et al.'s assumption of a uniform boundary-layer thickness is highly questionable.

The derivation of the momentum-integral equations for the boundary layers and the treatment of the inviscid core are described in the next section. Solutions to these equations and comparisons with experimental data are given in section 3. The principal conclusions are then given in section 4.

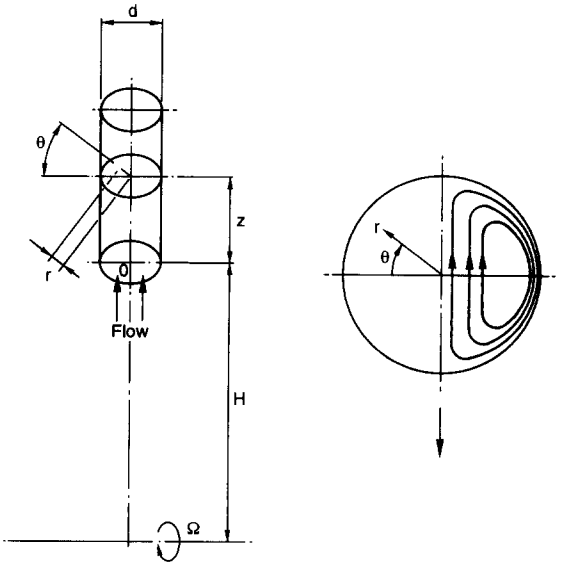

Figure 1 Coordinate system and schematic of secondary flow

2. The mathematical model

A rotating cylindrical coordinate system (r, Θ, z) is used as in Figure 1, with H denoting the distance of the origin from the axis of rotation. Velocity in this system is denoted (u, v, w), and nondimensional variables are defined as follows:

$$(U, V, W) = (u, v, w)/w_m$$
$$\sigma_{ij} = \tau_{ij} d/\mu w_m$$
$$x = 2r/d$$
$$P = \{p - [r^2 \sin^2\Theta + (H + z)^2]\rho\Omega^2/2\}/(\rho w_m^2/2) \quad (2)$$

Here τ_{ij} denotes the stress tensor components, including the laminar and turbulent contributions; μ denotes viscosity, p is static pressure, and ρ is density.

In fully developed flow it is assumed that axial gradients of velocity and stress vanish and the axial gradient of reduced pressure P is constant. Thus a nondimensional constant C is defined such that

$$C = -\frac{d\partial P}{\partial z} \quad (3)$$

The momentum conservation equations may then be written

$$\frac{U\partial U}{\partial x} + \frac{V}{x}\frac{\partial U}{\partial \Theta} - \frac{V^2}{x} - \frac{W}{\varepsilon}\sin\Theta = -\frac{1}{2}\frac{\partial P}{\partial x} + \frac{1}{Rx}\frac{\partial}{\partial x}(x\sigma_{rr}) \quad (4)$$

$$\frac{U\partial V}{\partial x} + \frac{V}{x}\frac{\partial V}{\partial \Theta} + \frac{UV}{x} - \frac{W}{\varepsilon}\cos\Theta = -\frac{1}{2x}\frac{\partial P}{\partial \Theta} + \frac{1}{Rx}\frac{\partial}{\partial x}(x\sigma_{r\Theta}) \quad (5)$$

$$\frac{U\partial W}{\partial x} + \frac{V}{x}\frac{\partial W}{\partial \Theta} + \frac{1}{\varepsilon}(U\sin\Theta + V\cos\Theta) = \frac{C}{4} + \frac{1}{Rx}\frac{\partial}{\partial x}(x\sigma_{rz}) \quad (6)$$

and the continuity equation gives

$$\frac{\partial}{\partial x}(xU) + \frac{\partial V}{\partial \Theta} = 0 \quad (7)$$

As is consistent with the usual boundary-layer assumptions, circumferential gradients of shear stress have been neglected in Equations 4 to 6.

For fully developed flow in a stationary duct (i.e., infinite ε) there is no secondary flow, the left-hand side of Equation 6 vanishes, and the pressure gradient is balanced by the shear-stress term on the right-hand side of Equation 6. This requires that shear-stress gradients are significant throughout the duct cross section. For flow in a rotating pipe, secondary velocities U and V are generated by the Coriolis terms in Equations 4 and 5. The left-hand side of Equation 6 is then nonzero, and for $R \gg 1$ the solution will have a boundary-layer form, the shear-stress terms only being significant in a region close to the wall. Separate treatments are appropriate for the core and boundary-layer regions, and these are described below. It will be assumed that the boundary-layer thickness is much smaller than the duct diameter and that the same thickness applies to both the axial and secondary velocity components.

2.1. The inviscid core

The equations for this region are obtained by neglecting the shear-stress terms in Equations 4 to 7. It is easy to see that an exact solution of these equations is

$$U = k\sin\Theta, \quad V = k\cos\Theta, \quad W = W_0 + \left(\frac{C}{4k} - \frac{1}{\varepsilon}\right)x\sin\Theta,$$
$$P = P_0 + \frac{Cz}{d} + \frac{2W_0}{\varepsilon}x\sin\Theta + \frac{1}{\varepsilon}\left(\frac{C}{4k} - \frac{1}{\varepsilon}\right)x^2\sin^2\Theta \quad (8)$$

where k, W_0, and P_0 are arbitrary constants. It is important to note that this is not the only possible solution. This solution was used by Mori and coworkers (1968, 1971) to describe the

Notation

C	Non-dimensional pressure gradient, Equation 3
C_{st}	Value of C for a stationary duct
d	Duct diameter
H	Distance of coordinates' origin from rotation axis
J	Constants, Equation 28
m	Secondary mass flow rate in boundary layer per unit length
M	Nondimensional flow rate $= m/\rho w_m d$
p	Static pressure
P	Reduced pressure, Equation 2
r	Radial coordinate
R	Reynolds number $= w_m d/\nu$
u	Radial velocity component
U	Nondimensional radial velocity $= u/w_m$
U^*	X-direction velocity component, Equation 13
v	Tangential velocity component
V	Nondimensional tangential velocity $= v/w_m$
V^*	Y-direction velocity component, Equation 13
w	Axial velocity component
w_m	Mean axial velocity
W	Nondimensional axial velocity $= w/w_m$
x	Nondimensional radial coordinate $= 2r/d$
X	Cartesian coordinate, Equation 13
Y	Cartesian coordinate, Equation 13
z	Axial coordinate

Greek symbols

α	$= R^{0.1}\varepsilon^{0.2}$
δ	Nondimensional boundary-layer thickness = dimensional thickness/$(d/2)$
ε	Rossby number $= w_m/\Omega d$
η	Boundary-layer coordinate $= (1 - x)/\delta$
Θ	Tangential coordinate
μ	Fluid viscosity
ν	Fluid kinematic viscosity $= \mu/\rho$
ρ	Fluid density
σ	Nondimensional stress tensor components, Equation 2
τ	Stress tensor components
Ω	Angular velocity of rotation

Superscripts

~	Values at the boundary-layer edge $\eta = 1$

core flow. In the present investigation, difficulties were encountered in trying to patch this solution to the boundary-layer solution, and it was concluded that this particular solution may be inappropriate for this problem. In Mori et al.'s work, the core flow was assumed to have the above form, but it was also assumed that the boundary-layer thickness did not vary with Θ, and variation with Θ of some other terms was neglected.

If it is assumed that the secondary velocities U and V are small in this region (compared to W), a general solution for the core flow may be obtained. To derive this solution it is useful to switch to a Cartesian coordinate system. Neglecting second-order terms in U and V and performing some algebraic manipulation, Equations 4 to 7 give, for the inviscid core,

$$\frac{\partial P}{\partial X} = 0 \tag{9}$$

$$\frac{\partial P}{\partial Y} = \frac{2W}{\varepsilon} \tag{10}$$

$$V^*\left(\frac{\partial W}{\partial Y} + \frac{1}{\varepsilon}\right) + U^*\frac{\partial W}{\partial X} = \frac{C}{4} \tag{11}$$

$$\frac{\partial U^*}{\partial X} + \frac{\partial V^*}{\partial Y} = 0 \tag{12}$$

where

$$X = x\cos\Theta, \qquad Y = x\sin\Theta \tag{13}$$

$$U^* = U\cos\Theta - V\sin\Theta, \quad V^* = U\sin\Theta + V\cos\Theta$$

Equations 9 and 10 imply that

$$\frac{\partial W}{\partial X} = 0 \tag{14}$$

Using this result and differentiating Equation 11, it follows that

$$\frac{\partial V^*}{\partial X} = 0 \tag{15}$$

With Equation 14, Equation 11 reduces to

$$\frac{\partial W}{\partial Y} = \frac{C}{4V^*} - \frac{1}{\varepsilon} \tag{16}$$

and using the fact that $U = 0$ on the symmetry plane $X = 0$, Equation 12 may be integrated to give

$$U^* = -\frac{X\partial V^*}{\partial Y} \tag{17}$$

If $m(\Theta)$ denotes the secondary mass flow rate in the boundary layer per unit length and $M = m/\rho w_m d$, then the condition that this flow is balanced by the mass flow across the core requires

$$(1-\delta)\cos\Theta[V^*]_{Y=(1-\delta)\sin\Theta} = -2M \tag{18}$$

where $\delta d/2$ is the boundary-layer thickness.

Converting back to the cylindrical coordinate system, neglecting first- and higher-order terms in δ, and considering values at the boundary-layer edge (denoted by a tilde), Equations 10, 16, and 18 give

$$\frac{d\tilde{P}}{d\Theta} = \frac{2\tilde{W}}{\varepsilon}\cos\Theta \tag{19}$$

$$\frac{d\tilde{W}}{d\Theta} = -\frac{\cos\Theta}{\varepsilon} - \frac{C}{8M}\cos^2\Theta \tag{20}$$

$$\cos\Theta(\tilde{U}\sin\Theta + \tilde{V}\cos\Theta) = -2M \tag{21}$$

From the continuity equation it also follows that

$$\tilde{U} = 2\frac{dM}{d\Theta} \tag{22}$$

A similar core solution to this was derived by Ito and Nanbu (1971) in their laminar flow analysis. However, with these workers' approximations, the term involving $1/\varepsilon$ in Equation 20 would be neglected.

2.2. The momentum-integral equations for the boundary layer

The boundary-layer equations are obtained from Equations 4 to 7, assuming that $\delta \ll 1$. The validity of this assumption will be further discussed later. With the usual boundary-layer assumptions, the radial momentum equation reduces to

$$\frac{\partial P}{\partial x} = 0 \tag{23}$$

The following boundary-layer velocity profiles are assumed:

$$W = \tilde{W}(\Theta)g(\eta)$$

$$V = V_0(\Theta)f(\eta) \tag{24}$$

where V_0 is an unspecified function of Θ, and

$$\eta = (1-x)/\delta, \quad g(\eta) = \eta^{1/7}, \quad f(\eta) = (1-\eta)\eta^{1/7} \tag{25}$$

These profiles are similar to those used in momentum-integral solutions for rotating disc flows, which were first introduced by von Karman (1921). Note that the appropriate boundary conditions for W and V at $\eta = 0$ and 1 are approximately satisfied by this choice of profile, since for $\delta \ll 1$ it follows that $\tilde{V} \ll V_0$.

Integrating Equations 5 and 6 from $\eta = 0$ to 1 using Equations 23 to 25 and the assumption $\delta \ll 1$ and $\delta \ll \varepsilon$ gives, after some algebraic manipulation,

$$2J_{ff}V_0\frac{dV_0}{d\Theta} + \frac{1}{2}\frac{d\tilde{P}}{d\Theta} - \frac{J_g\tilde{W}\cos\Theta}{\varepsilon} + \frac{J_{ff}V_0^2}{\delta}\frac{d\delta}{d\Theta} = \frac{\sigma_{r\Theta,w}}{\delta R} \tag{26}$$

$$\tilde{W}(J_{fg} - J_f)\frac{dV_0}{d\Theta} + J_{fg}V_0\frac{d\tilde{W}}{d\Theta} - (J_{fg} - J_f)\frac{V_0}{\delta}\frac{\tilde{W}d\delta}{d\Theta} + \frac{J_fV_0\cos\Theta}{\varepsilon} - \frac{C}{4} = \frac{\sigma_{rz,w}}{\delta R} \tag{27}$$

where the subscript w denotes a value at the wall and the J's are constants with the following values.

$$J_f = 0.408333, \quad J_g = 0.875,$$

$$J_{ff} = 0.207126, \quad J_{fg} = 0.340278 \tag{28}$$

Integrating across the boundary layer to find the secondary mass flow rate in the boundary layer gives

$$M = \delta V_0 J_f/2 \tag{29}$$

Blasius law is used to estimate the wall shear stress and, using similar assumptions to those of von Karman and others for rotating disc flows, $\sigma_{rz,w}$ and $\sigma_{r\Theta,w}$ are given by

$$\sigma_{rz,w} = -0.02676R^{0.75}\tilde{W}(V_0^2 + \tilde{W}^2)^{0.375}/\delta^{0.25} \tag{30}$$

$$\sigma_{r\Theta,w} = V_0\sigma_{rz,w}/\tilde{W} \tag{31}$$

A further useful relationship is obtained by integrating across the duct area to find the axial flow rate and using the definition

of w_m. This gives for $\delta \ll 1$

$$\int_{-\pi/2}^{\pi/2} \tilde{W} \cos^2 \Theta \, d\Theta = \pi/2 \tag{32}$$

3. Solutions

The momentum-integral equations (Equations 26 and 27) with the auxiliary relations (Equations 28 to 32), plus the core equations (Equations 19 to 22), define the mathematical problem for calculating the flow field. The independent variables of the problem are R, ε, and Θ. The dependent variables are C, $\tilde{W}(\Theta)$, $V_0(\Theta)$, $\tilde{V}(\Theta)$, $\tilde{U}(\Theta)$, $M(\Theta)$, $\tilde{P}(\Theta)$, $\delta(\Theta)$, $\sigma_{rz,w}(\Theta)$, and $\sigma_{r\Theta,w}(\Theta)$. Solutions to this system are described below.

3.1. The limiting conditions $\varepsilon \ll 1 \ll R$

For these conditions an analytical solution is possible, analogous to Owen et al.'s (1985) linear turbulent Ekman layer solution.

Neglecting higher-order terms, Equations 26 and 27 with Equations 19, 30, and 31 reduce to

$$(1 - J_g)\tilde{W} \cos \Theta/\varepsilon = -0.02676 V_0 (V_0^2 + \tilde{W}^2)^{0.375}/(R^{0.25}\delta^{1.25}) \tag{33}$$

$$J_f V_0 \cos \Theta/\varepsilon = -0.02676 \tilde{W} (V_0^2 + \tilde{W}^2)^{0.375}/(R^{0.25}\delta^{1.25}) \tag{34}$$

From Equations 20 and 29, it may be deduced that

$$\varepsilon C \cos \Theta/4 = -J_f \delta V_0 \tag{35}$$

Equations 32 to 35 may be solved to give C, $\tilde{W}(\Theta)$, $V_0(\Theta)$, and $\delta(\Theta)$ in terms of ε and R. Using Equations 28 for the J coefficients, it is straightforward to show that this solution is

$$\begin{aligned} \tilde{W} &= A \cos^{1.125}\Theta \\ V_0 &= -0.5533\tilde{W} \\ \delta &= 0.1966 A^{0.6} \varepsilon (\varepsilon R)^{-0.2} \cos^{-0.125} \Theta \\ C &= 0.1777 A^{1.6} (\varepsilon R)^{-0.2} \end{aligned} \tag{36}$$

where

$$A = \pi \Big/ \int_{-\pi}^{\pi} \cos^{3.125} \Theta \, d\Theta \tag{37}$$

In deriving the momentum integral equations, it was assumed that $\delta \ll \varepsilon$. The above solution is consistent with this assumption, provided $(\varepsilon R)^{0.2}$ is large. Hence, the range of applicability may be restricted to $1 \ll 1/\varepsilon \ll R$. Of course, in the region of $\Theta = \pi/2$ and $-\pi/2$, the boundary-layer assumptions will not be valid, and some local departures from this solution are to be expected.

3.2. The limiting conditions $1 \ll \varepsilon \ll R$

For these conditions, Equation 20 reduces to

$$\frac{d\tilde{W}}{d\Theta} = -\frac{C \cos^2 \Theta}{8M} \tag{38}$$

From order-of-magnitude considerations, it might be expected that $V_0 \ll 1$. The momentum equations (Equations 26 and 27), using Equations 19, 30, and 31, may therefore be written

$$2J_{ff}V_0 \frac{dV_0}{d\Theta} + (1 - J_g)\frac{\tilde{W}}{\varepsilon} \cos \Theta + \frac{J_{ff}V_0^2}{\delta}\frac{d\delta}{d\Theta} = -\frac{0.02676}{\delta(\delta R)^{0.25}} V_0 |\tilde{W}|^{0.75} \tag{39}$$

$$\tilde{W}(J_{fg} - J_f)\frac{dV_0}{d\Theta} + J_{fg}V_0 \frac{d\tilde{W}}{d\Theta} - (J_{fg} - J_f)\frac{V_0}{\delta}\frac{\tilde{W}d\delta}{d\Theta} = -\frac{0.02676}{\delta(\delta R)^{0.25}} \tilde{W}|\tilde{W}|^{0.75} \tag{40}$$

It is convenient to define $\alpha = R^{0.2}\varepsilon^{0.1}$. Inspection of Equations 38 to 40 with Equations 29, 32, 19, 21, and 22 shows that a solution is possible in which αC is constant and $\tilde{W}$, $V_0\sqrt{\varepsilon}$, $\alpha\delta/\sqrt{\varepsilon}$, αM, $\tilde{P}\varepsilon$, $\alpha\tilde{V}$, $\alpha\tilde{U}$, $\alpha\sigma_{r\Theta,w}/R$, and $\alpha\sigma_{rz,w}/R$ are functions of Θ only.

The first-order differential equations (Equations 38 to 40 and Equation 19) were solved numerically using a variable step gear method, as implemented in a mathematical subroutine library. The solution starts at the trailing edge $\Theta = \pi/2$ and marches in the direction of the boundary-layer flow to the leading edge at $\Theta = -\pi/2$. In addition to the Reynolds number R and Rossby number ε, starting values of δ, V_0, and $\tilde{W}$ and of the pressure gradient C must be specified in this solution. V_0 at $\Theta = \pi/2$ was set to a very small value (typically 10^{-8}) to ensure that the initial mass flow in the boundary layer was very small. The solution was then found to be insensitive to the starting value of δ, which was set to be of order $R^{-0.2}$; a rapid readjustment of δ then occurred close to $\Theta = \pi/2$. An iterative technique was used to find values of $\tilde{W}$ at $\Theta = \pi/2$ and C for which both Equation 32 and the condition that the boundary-layer mass flow at $\Theta = \pi/2$ must be zero were satisfied.

The numerical solution is shown in Figure 2. According to

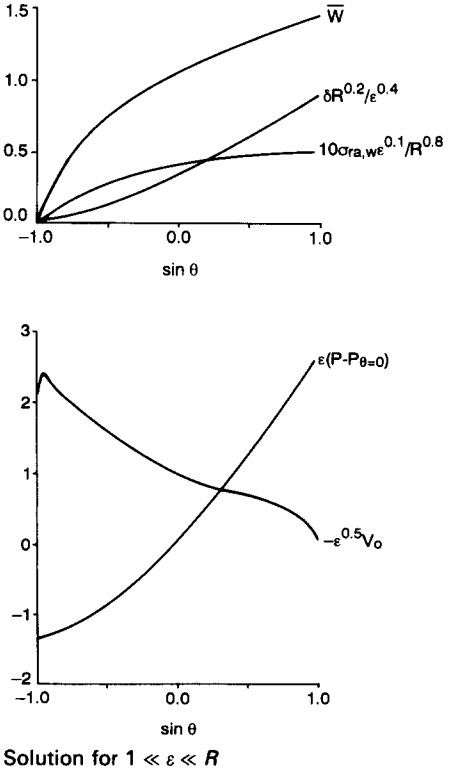

Figure 2 Solution for $1 \ll \varepsilon \ll R$

the solution, the nondimensional pressure gradient is given by

$$C = 0.268\varepsilon^{-0.1}R^{-0.2} \tag{41}$$

If C_{st} denotes the pressure drop coefficient for a stationary pipe given by the Blasius formula, this result may be written

$$C/C_{st} = 0.878\varepsilon^{-0.1}R^{0.05} \tag{42}$$

3.3. Comparison with measurements

In this section the solution given in section 3.2 and numerical solutions of the equations given in section 2 (assuming $\delta \ll 1$) are compared with Ito and Nanbu's (1971) measurements for fully developed flow in a circular duct. The numerical solutions were obtained using a similar method to that described in section 3.2.

Figure 3 shows the increase in the pressure drop coefficient due to rotation. Ito and Nanbu correlated their results against R/ε^2. For $15 \leq R/\varepsilon^2 \leq 500$, they give the correlation

$$C/C_{st} = 0.924\varepsilon^{-0.1}R^{0.05} \tag{43}$$

Some correspondence between this result and the limiting solution (Equation 42) is clear. Computed solutions at finite values of R and ε indicate that the value of R/ε^2 does not uniquely define C/C_{st}; there is an additional, relatively small Reynolds number effect. It is quite possible that in the experiments, which only covered a limited range of R, this effect could have been missed. The values of R of 5×10^3 and 10^5 for which numerical solutions are given are roughly representative of the experimental range. It should be noted that the numerical results were obtained by integrating the shear stress over the duct surface using the calculated solution for velocities and boundary-layer thickness. Owing to the assumptions made in the analysis not being strictly valid for these conditions, these differed from the values of C specified in the governing equations. In particular, when calculating the core flow, no account is taken of the reduction in cross-section area due to the boundary layer, so there is some double accounting of the specified pressure gradient over the boundary-layer regions. Discrepancies of the order of 20% in this overall force balance were observed; these are consistent with the values calculated for δ given below.

Figure 4 gives a comparison between theory and Ito and Nanbu's measurements of axial velocity on the symmetry plane and the circumferential variation of pressure at the pipe wall. The predicted boundary-layer thickness at the leading and trailing edges is also indicated in Figure 4a; these appear to be in good agreement with measurement. Clearly the assumption $\delta \ll 1$ is highly questionable for these conditions. Discrepancies between theory and experiment near the trailing edge can be attributed to the relatively large boundary-layer thickness in this region. The differences near the leading edge are more difficult to explain, since δ is small in this region. Since the local Reynolds number will be lower in this region, it is possible that the assumed 1/7th power laws are inappropriate here, or even that the flow is locally laminar.

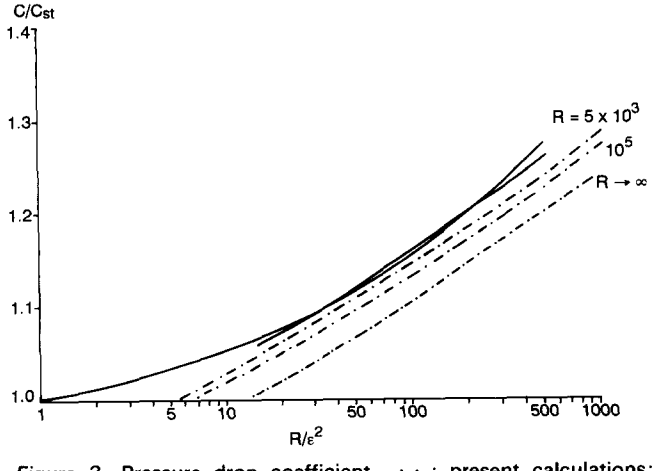

Figure 3 Pressure drop coefficient. –·–·–: present calculations; ———: experimental measurements (Ito and Nanbu 1971)

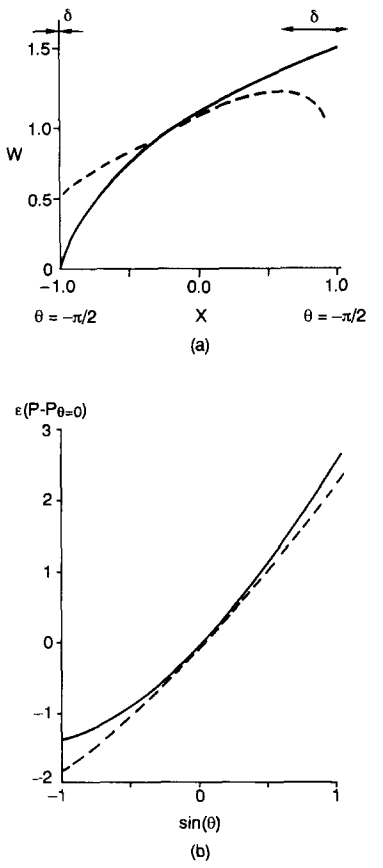

Figure 4 Results for $R = 2.5 \times 10^4$, $\varepsilon = 25$. (a) Axial velocity on symmetry plane; (b) circumferential variation of pressure. ———: present calculations; – – –: experimental correlations (Ito and Nanbu 1971)

3.4. Range of validity of the model

It is of interest to consider under what conditions the above analysis is likely to be valid. In deriving the mathematical model it was assumed that the secondary velocity in the core was relatively small and that the boundary layer was very thin. These two assumptions can be justified if $\varepsilon V^{*2} \ll 1$ and $\delta \ll 1$. Calculations were performed to see for what range of ε and R these conditions are satisfied. Problems with convergence of the numerical solution algorithms were encountered for small values of ε, and so attention here is confined to $\varepsilon \geq 1$.

Figure 5 shows the computed values of εV^{*2} and δ at $\Theta = 0$ for various values of ε and R. The hatched area on these graphs denotes the parameter range $10 \leq \varepsilon \leq 100$, $10^4 \leq R \leq 10^5$, which is representative of engine conditions. These results confirm that εV^{*2} is small, but indicate that the assumption $\delta \ll 1$ will only be valid for very high Reynolds number flow.

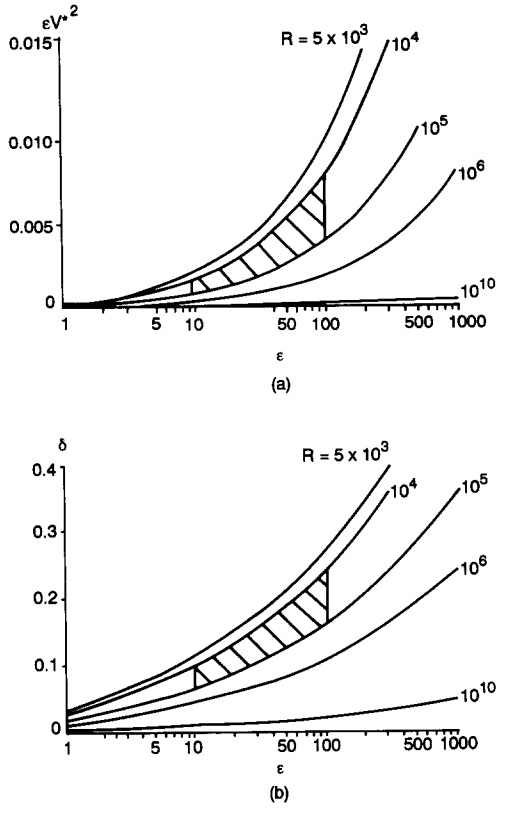

Figure 5 Solution at $\Theta = 0$. (a) Core secondary velocity εV^{*2}; (b) boundary-layer thickness δ. Hashed areas are typical engine parameter range

4. Conclusions

A momentum-integral method, previously used for rotating disc flows, has been applied to the problem of fully developed flow in a circular duct rotating about an orthogonal axis. It is assumed that the secondary velocities in the inviscid core are small (relative to the axial velocity) and that the boundary-layer thickness is much less than the duct diameter. An analytical solution is derived for the limiting conditions $1 \ll 1/\varepsilon \ll R$, and a solution for $1 \ll \varepsilon \ll R$ is found using numerical methods. Numerical methods are also used to obtain solutions of the equations for finite values of ε and R. Although the solutions are valid for both radial inflow and outflow, attention has been centered on radial outflow, for which some experimental data are available.

Good qualitative and some quantitative agreement between the momentum-integral solution and Ito and Nanbu's (1971) pressure drop measurements was found. For $1 \ll \varepsilon \ll R$, the solution predicts the pressure drop coefficient divided by the stationary tube value to be $0.878\varepsilon^{-0.1}R^{0.05}$, compared with Ito and Nanbu's empirical correlation $0.924\varepsilon^{-0.1}R^{0.05}$. Solutions of the integral model for values of R and ε comparable to the experimental range indicate a dependency on Reynolds number that was not observed experimentally, possibly due to only a limited parameter range being investigated experimentally. Differences between the theory and measurements are attributed, at least in part, to the assumption of very small boundary-layer thickness. The calculations suggest that the boundary-layer thickness will only be negligibly small for Reynolds numbers much higher than those representative of turbine blade cooling passages.

The circumferential variation of pressure on the duct wall is in reasonable agreement with Ito and Nanbu's measurements, some discrepancies being evident near the leading side. The axial velocity profiles show further departure from the measurements. Near the trailing edge, these can be attributed to the relatively thick boundary layer in this region. Near the leading edge, the local Reynolds number is lower, and it is likely that the assumed velocity and shear stress relations are not valid. The flow may even be laminar in the vicinity of the leading edge. Predicted boundary-layer thicknesses are consistent with the velocity measurements.

Acknowledgments

The assistance of Mr. P. D. Clark with the numerical solution is gratefully acknowledged.

References

Benton, G. S. and Boyer, D. 1966. Flow through a rapidly rotating conduit of arbitrary cross-section. *J. Fluid Mech.*, **26**, 69–79

Chew, J. W. 1990. Prediction of rotating disc flow and heat transfer in gas turbine engines. *Proc. Third Int. Symp. Transport Phenomena and Dynamics of Rotating Machinery, Hawaii*, Hemisphere Corp., 145–160

Greenspan, H. P. 1968. *The Theory of Rotating Fluids.* Cambridge University Press, Cambridge, UK

Iacovides, H. and Launder, B. E. 1987. Turbulent momentum and heat transport in square-sectioned ducts rotating in orthogonal mode. *Numer. Heat Transfer*, **12**, 475–491

Ito, H. and Nanbu, K. 1971. Flow in rotating straight pipes of circular cross section. *ASME J. Basic Eng.*, 383–394

von Karman, T., 1921. Uber laminare und turbulente reibung. *Z. Angew. Math. Mech.*, **1**, 233–252

Mori, Y., Fukada, T., and Nakayama, W. 1971. Convective heat transfer in a rotating radial circular pipe (2nd report). *Int. J. Heat Mass Transfer*, **14**, 1807–1824

Mori, Y. and Nakayama, W. 1968. Convective heat transfer in rotating radial circular pipes (1st report, laminar region). *Int. J. Heat Mass Transfer*, **11**, 1027–1040

Morris, W. D. 1981. *Heat Transfer and Fluid Flow in Rotating Coolant Channels.* Research Studies Press, Letchworth, UK

Owen, J. M., Pincombe, J. R., and Rogers, R. H. 1985. Source-sink flow inside a rotating cylindrical cavity. *J. Fluid Mech.*, **155**, 233–265

Taylor, C., Xia, J. Y., Medwell, J. O., and Morris, W. D. 1991. Finite element modelling of flow and heat transfer in turbine blade cooling ducts. I. Mech. E. paper C423/037